Macromolecules

pubs.acs.org/Macromolecules Article

Unveiling Local Dynamics of a Triptycene-Based Porous Polymer by Solid-State NMR

Elisa Della Latta,[#] Kayla R. Storme,[#] Molly C. Warndorf, Alfredo Alexander-Katz, Silvia Borsacchi, Francesca Martini,* Timothy M. Swager,* and Marco Geppi

Cite This: *Macromolecules* 2024, 57, 11152−11165 Read Online

ACCESS | Metrics & More | Article Recommendations | Supporting Information

ABSTRACT: Membrane-based technologies for gas separation and capture are promising low-energy alternatives to the most common energy-consuming processes such as distillation and absorption. In this frame, porous polymers are attracting considerable interest, but issues related to a trade-off between permeability and selectivity as well as to the long-term stability of the membrane performances need to be overcome. To this end, the study of local dynamics is crucial as it directly correlates with the transport and separation characteristics of polymer-based membranes while also shedding light on plasticization and physical aging phenomena. This work presents a comprehensive characterization of the dynamic properties of a triptycene-based porous polymer with potential application in membrane-based gas separation technology by means of molecular dynamics (MD) simulations and solid-state NMR (SSNMR). The investigated polymer has triptycene-based structural repeating units bearing *t*-butyl groups that are connected by perfluorinated biphenyl repeats. The combination of different SSNMR variable temperature experiments including measurements of ^{1}H, ^{13}C, and ^{19}F spin−spin and spin−lattice relaxation times, $^{1}H-^{13}C$ and $^{19}F-^{13}C$ dipolar chemical shift correlation experiments, and ^{2}H experiments provided selective and detailed information on the molecular motions involving the *t*-butyl, triptycene, and perfluorinated biphenyl groups. A synergistic analysis of the acquired data, employing theoretical dynamic models and comparisons with MD simulations and calculated potential energy scans (PES), has enabled the determination of motion parameters, including activation energies and correlation times. This approach also yielded insights into the motion amplitudes and geometry. These findings can be valuable for future research aimed at elucidating the molecular origins of membrane performance, not only for the polymer under investigation but also for similar polymer-based membranes.

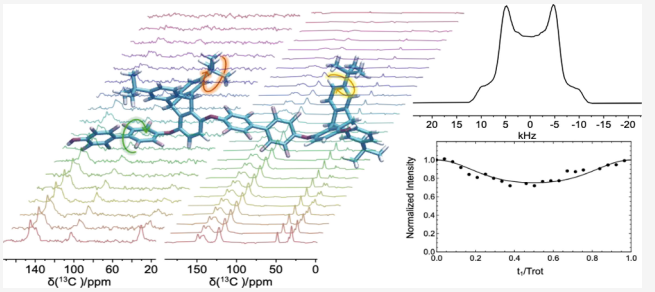

1. INTRODUCTION

Membrane-based gas separations have garnered considerable interest as energy-efficient alternatives to conventional thermal separations.[1−3] Although polymer membranes are used in some industrial separations, such as hydrogen recovery and removal of CO_2 from natural gas, their broader adoption is limited by an apparent trade-off between gas permeability and selectivity described by the Robeson upper bound.[4] Fluoropolymers are promising candidates for membrane materials because they exhibit the highest separation performance to date, often defining the upper-bound limits for several gas pairs, which is attributed to fluorine-enhanced polymer−penetrant interactions. Some investigations have probed the influence of fluorination on sorption and gas transport,[5−8] yet the impact of polymer−penetrant interactions is relatively understudied due to the limited fluorinated structures available for testing.[9,10] Nucleophilic aromatic substitution (S_NAr) is a promising method used to synthesize several fluorinated aryl ether (FLARE) polymers that demonstrate desirable long-term chemical, structural, and thermal stabilities.[11−13] Among these is the intrinsically porous triptycene-containing FLARE polymer first synthesized by Long et al. that is the focus of this study.[14]

Molecular mobility on the picosecond time scale can play a pivotal role in gas transport within porous polymers. Indeed, rapid local reorientations, such as reorientational motions of *t*-butyl groups and phenyl rings, may dynamically open or close bottlenecks between the free volume elements of the pore network. Dynamics can also be an indirect probe of undesired phenomena, such as physical aging densification[15] and plasticization.[16,17] Hence, investigating dynamics is paramount for comprehending the permselectivity of membrane polymers toward various gases and elucidating the transport mechanism.

Received: October 29, 2024
Accepted: November 20, 2024
Published: November 29, 2024

Scheme 1. Synthesis of the Deuterated Monomer (Compound 2) and of the Deuterated Polymer C1-d18

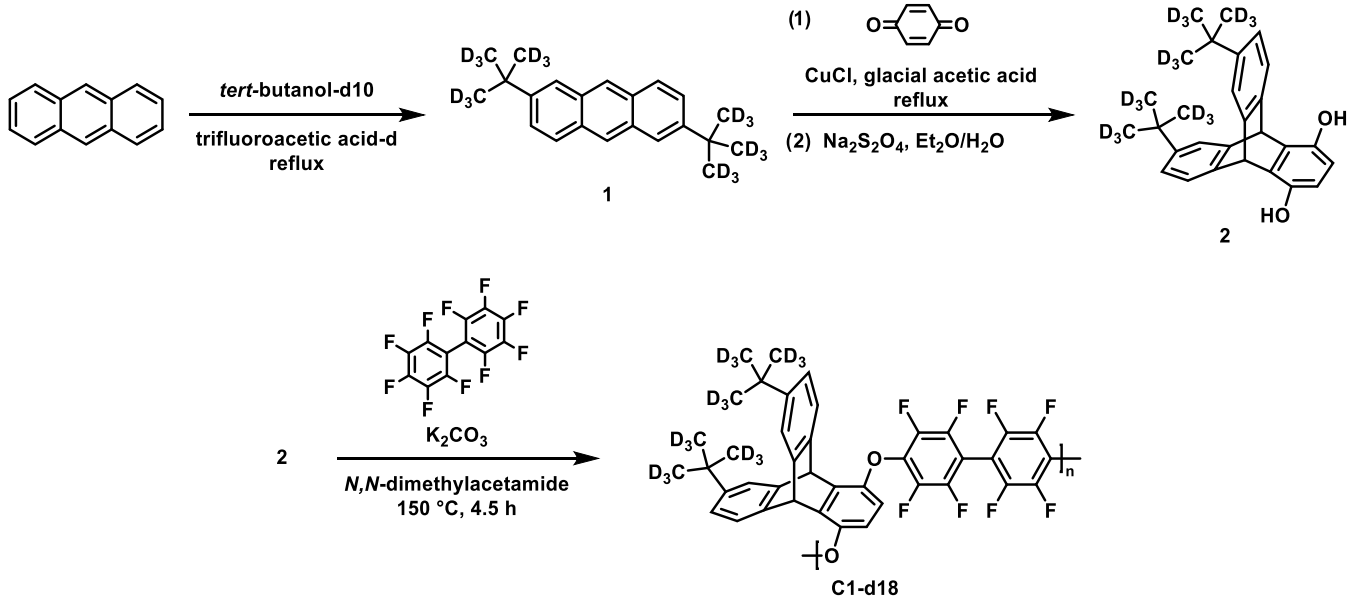

Furthermore, this offers insights into the long-term stability of these systems. In the field of porous materials, the role of dynamics has been extensively investigated in metal organic frameworks (MOFs), where the motions of aromatic rings are fundamental to molecular rotor engineering[18,19] and were found to be strictly coupled to the passage of guest molecules.[20−22] However, research on molecular motions in porous polymers and their correlation with gas sorption, transport, physical aging, and plasticization phenomena remains limited.[23−26]

Solid-state NMR spectroscopy (SSNMR) offers a diverse set of tools to investigate molecular dynamics across various time scales, ranging from seconds to picoseconds. Spin−lattice relaxation times (T_1) are highly sensitive to reorientational motions in the fast MHz frequency regime. Analyzing their trends with temperature using semiempirical dynamic models enables the determination of characteristic motion parameters such as the activation energy and correlation times. Additionally, measuring anisotropic interactions, such as ^{13}C chemical shift anisotropy, ^{2}H quadrupolar interactions, and dipolar couplings, provides information not only on the time scale but also on the geometry of the motions. Recently, SSNMR has been utilized to study both host[21,27−29] and guest[30,31] dynamics in MOFs. Furthermore, T_1 measurements have been employed to investigate the impact of physical aging[15,16] and CO_2-induced plasticization[17] on chain mobility[32,33] in porous polymers.

SSNMR studies can greatly benefit from comparison with computational analysis, which offers supplementary insights and facilitates the interpretation of the experimental results. Recently, researchers have leveraged molecular dynamics (MD) simulations to gain detailed information on the molecular structure and pore morphology of polymers at minimal computational cost.[34−38] Models have been used to identify structural adjustments to increase the rigidity of polymers and estimate relevant properties such as pore size distributions, fractional free volume (FFV), and surface area.[35,39−43] Advances in modeling and accessibility to modeling techniques enabled recent studies that explore the gas transport mechanisms and sorption behavior of gases through different polymer materials.[44,45]

In this study, we present a thorough characterization of the dynamic properties of a FLARE polymer containing triptycene units by employing SSNMR and MD simulations. The polymer under investigation consists of triptycene-based structural units linked by perfluorinated biphenyl groups. A variant featuring deuterated *t*-butyl groups was also studied. We delved into the reorientational motions involving the perfluorinated biphenyl linkers, *t*-butyl groups, and triptycene thanks to the synergistic analysis of data arising from various SSNMR techniques by using theoretical dynamic models. Specifically, our methodology encompasses measurements and analyses of ^{1}H, ^{19}F, and ^{13}C relaxation times, $^{1}H-^{13}C$ dipolar chemical shift (DIPSHIFT) correlation experiments,[46,47] and ^{2}H static spectra. By integrating these experimental findings with computational analyses, we not only extract quantitative information on motion parameters such as activation energy and correlation times but also elucidate the amplitude of the motions.

To the best of our knowledge, this study is among the first detailed investigations of the local dynamics of porous polymers. The work offers new and valuable insights into the local dynamics of triptycene and perfluorinated biphenyl groups, which, along with others that share similar structural features, are commonly employed as building blocks or linkers in various porous materials. The insights gained from this research could be instrumental in future studies aimed at exploring the molecular origin of the gas separation performances of the examined polymers or similar systems, which may be influenced by these molecular motions.

2. MATERIALS AND METHODS

2.1. Materials. All materials were used as received unless otherwise noted. Decafluorobiphenyl was purchased from Alfa Aesar (Ward Hill, MA) and recrystallized in hexanes before use. Anhydrous *N*,*N*-dimethylacetamide, acetone, and ethyl acetate were purchased from Sigma-Aldrich Co. (St. Louis, MO). Hexanes and methanol were purchased from Macron Fine Chemicals (Radnor, PA). Hydrochloric acid (37%) solution in water was purchased from Sigma-Aldrich Co.

https://doi.org/10.1021/acs.macromol.4c02666
Macromolecules 2024, 57, 11152−11165

Table 1. Molecular Weight (M_n) and Molecular Weight Distribution (PDI) Obtained from Size Exclusion Chromatography (SEC) and Glass-Transition Temperature Measured by Differential Scanning Calorimetry (DSC) of Polymers C1 and C1-d18

Polymer	M_n (kDa)	PDI	T_g (°C)
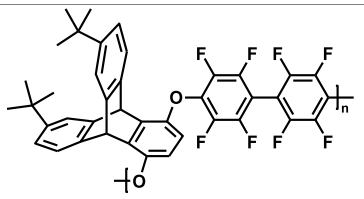 C1	32.4	1.8	298
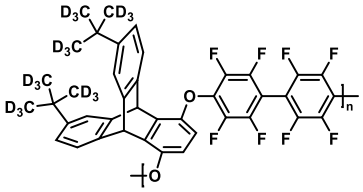 C1-d18	31.9	1.3	296

(St. Louis, MO) and diluted with deionized water to make a 3 M solution. 6,11-Di(*tert*-butyl)triptycene-1,4-hydroquinone was purchased from Akita Innovations (North Billerica, MA) and purified via recrystallization with ethyl acetate and hexanes. N_2 used for testing was ultrahigh purity from Airgas.

2.1.1. Preparation of the Deuterated Monomer. The synthesis of the deuterated monomer is depicted in Scheme 1. Anthracene (4.7766 g, 26.8 mmol) and *tert*-butanol-d_{10} (7.6 mL, 80.6 mmol) were added to a flame-dried Schlenk flask with trifluoroacetic acid-*d* (33.5 mL) under argon. A reflux condenser was fitted onto the flask, and the solution was refluxed for 23 h before treating with solid sodium bicarbonate. The black crude mixture was washed with deionized water (200 mL) and hexanes (400 mL). The organic phase was separated before diluting with methylene chloride to obtain a clear solution and drying over sodium sulfate. Solids were filtered and discarded. The organic solvent was removed under reduced pressure. The resulting solids were recrystallized in hexanes and washed with a small amount of cold hexanes to yield compound **1** as a white solid (4.0892 g, 49%). HRMS (DART-TOF$^+$) (high-resolution mass spectrometry, direct analysis in real-time, time-of-flight): mass $[M]^+$ calculated for $C_{22}H_8D_{18}$ 308.31588 Da, measured 308.31441 Da.

Compound **1** (3.7500 g, 12.15 mmol) and *p*-benzoquinone (6.3977 g, 59.19 mmol) were added to a flame-dried Schlenk flask with glacial acetic acid (65 mL). Copper(I) chloride (1.1791 g, 11.91 mmol) was added to the flask before fitting with a reflux condenser. The solution was refluxed for 3.5 h. Once cooled to room temperature, the dark brown solution was quenched by pouring it into ice water. The precipitate was collected on filter paper, washed with hot water, dissolved in methylene chloride, and purified with a silica gel plug that was flushed with methylene chloride. The solvent was removed *in vacuo* to give an orange solid that was redissolved in 100 mL of diethyl ether. A 100 mL solution of deionized water with excess sodium dithionite was poured into the flask and stirred vigorously until the solution turned pale yellow. The organic layer was separated before extracting the aqueous layer with ethyl ether. All organic extracts were combined, washed with water and brine, dried over sodium sulfate, and filtered. The solvent was removed *in vacuo* to yield compound **2** as a tan solid (1.9899 g, 40%). HRMS (DART-TOF$^+$): mass $[M + H]^+$ calculated for $C_{28}H_{13}O_2D_{18}$ 417.34484 Da, measured 417.34499 Da.

2.1.2. Synthesis of Polymers. The polymerization of **C1** was carried out using a modified version of a previously published procedure.[14] The same polymerization scheme was used for **C1-d18**, as sketched in Scheme 1. Compound **2** (500.0 mg, 1.2 mmol) and decafluorobiphenyl (400.9 mg, 1.2 mmol) were sealed in a flame-dried Schlenk flask. The flask was evacuated and backfilled with argon three times before the solids were dissolved in 18.75 mL of anhydrous *N*,*N*-dimethylacetamide. Potassium carbonate (382.0 mg, 2.8 mmol) was charged into the pale yellow solution. The solution was heated with stirring to 150 °C for 4.5 h resulting in a dark brown solution. After cooling the solution to 80 °C, the polymer was precipitated into boiling acidic (HCl) water (pH ∼2−3) to remove salts and lower-molecular-weight oligomers. The precipitate was collected using vacuum filtration and dried briefly. The solids were dissolved in *N*,*N*-dimethylacetamide and precipitated again into boiling acidic HCl (pH ∼2−3). After the precipitate was collected using vacuum filtration, the polymer was dissolved in acetone and precipitated into deionized water to remove *N*,*N*-dimethylacetamide. The precipitate was collected using vacuum filtration and dried under vacuum at 120 °C overnight to yield a white powder (455.5 mg). The molecular weight (M_n), molecular weight distribution (PDI), and glass-transition temperature (T_g) of **C1** and **C1-d18** are reported in Table 1.

2.2. Polymer Characterization. *2.2.1. Size Exclusion Chromatography (SEC).* SEC was performed using an Agilent 1260 Infinity system with a guard column (Agilent PLgel; 5 μm; 50 × 7.5 mm^2) and three analytical columns (Agilent PLgel; 5 μm; 300 × 7.5 mm^2; 10^5, 10^4, and 10^3 Å pore sizes). Samples with concentrations ≤1.0 mg mL^{-1} were prepared in HPLC-grade tetrahydrofuran and analyzed at a 1.0 mL min^{-1} flow rate and 35 °C. The instrument was calibrated with polystyrene standards between 1.7 and 3150 kg mol^{-1}. Molecular weight values were calculated using ChemStation GPC Data Analysis Software (rev B.01.01) based on the refractive index signal.

2.2.2. Differential Scanning Calorimetry (DSC). Cyclic DSC measurements were performed twice for each polymer sample using a DSC 250 from TA Instruments between 30 and 375 °C at a heating and cooling rate of 10 °C min^{-1}. Polymer T_g's were determined from the second scan, using TA Instruments TRIOS glass-transition analysis software (version 5.1.1).

2.2.3. Brunauer−Emmett−Teller (BET) Surface Area. BET surface areas of polymer samples were measured at 77 K using N_2 sorption using a Micromeritics 3Flex analyzer. All samples were degassed under high vacuum at 200 °C for at least 24 h prior to analysis.

2.3. Solid-State NMR Experiments. High-resolution solid-state NMR experiments were carried out on a Bruker Avance Neo spectrometer working at Larmor frequencies of 500.13, 125.77, 470.59, and 76.77 MHz for ^{1}H, ^{13}C, ^{19}F, and ^{2}H, respectively.

^{19}F magic angle spinning (MAS) spectra were recorded at a MAS frequency of 55 kHz by means of a double-channel (H/F-X) cross-polarization (CP)/MAS probe for rotors with an outer diameter of 1.3 mm. The ^{19}F pulse duration was 1.9 μs. A recycle delay of 5 s was used, and 256 scans were accumulated.

https://doi.org/10.1021/acs.macromol.4c02666
Macromolecules 2024, 57, 11152−11165

^{1}H, ^{19}F, ^{13}C, and ^{2}H experiments were carried out by means of a double-channel (H/F-X) CP/MAS probe for rotors with an outer diameter of 4 mm. The ^{1}H, ^{19}F, ^{13}C, and ^{2}H 90° pulse durations were 3.85, 3.10, 3.90, and 6 μs, respectively.

^{1}H and ^{13}C spectra were acquired at a MAS frequency of 15 kHz. ^{1}H MAS spectra were recorded using 4 scans and a recycle delay of 2 s. ^{1}H−^{13}C and ^{19}F−^{13}C CP/MAS spectra were acquired by applying high-power decoupling from either protons or fluorine atoms during signal acquisition using the SPINAL-64 scheme.[48] ^{1}H−^{13}C CP/MAS spectra were obtained using contact times (ct) of 0.1, 0.5, and 1 ms recording 2600−4000 scans, while ^{19}F−^{13}C CP/MAS experiments were performed using ct of 0.5, 2, and 7 ms and accumulating 8000 scans. Two-dimensional ^{19}F−^{13}C FSLG (frequency-switched Lee−Goldburg)-HETCOR (HETeronuclear CORrelation)[49] experiments were performed using a ct of 0.5 ms, acquiring 64 rows and 360 scans. ^{1}H−^{13}C and ^{19}F−^{13}C dipolar chemical shift (DIPSHIFT) correlation[46,47] experiments were carried out using a MAS frequency of 6 kHz, acquiring 200−504 scans with a recycle delay of 2 s for each of the 24 increments of the evolution time. For ^{1}H−^{13}C and ^{19}F−^{13}C DIPSHIFT experiments, ct values of 1 and 0.5 ms were used, respectively.

Static ^{2}H spectra were obtained using the quadrupolar echo pulse sequence using an echo delay of 16 μs and recording 64 scans with a recycle delay of 2 s.

^{13}C spin−lattice relaxation times (T_1) were measured in the range of temperature 10−100 °C, by the Torchia pulse sequence,[50] exploiting either ^{19}F−^{13}C CP or ^{1}H−^{13}C CP for carbons belonging to biphenyl and triptycene units, respectively. ^{13}C T_1's via ^{19}F−^{13}C CP were obtained with ct = 5 ms and a recycle delay of 2 s using a variable recovery delay ranging from 0.01 to 25 s. ^{13}C T_1's via ^{1}H−^{13}C CP were obtained with a contact time of 1 ms and a recycle delay of 2 s using a variable recovery delay ranging from 0.01 to 40 s. In both cases, 360 scans were acquired for each delay. The sample temperature was calibrated by measuring the ^{207}Pb chemical shift of $Pb(NO_3)_2$ at a MAS frequency of 15 kHz in order to take into account the effect of frictional heating due to sample spinning. ^{1}H and ^{19}F T_1's at the Larmor frequencies of 500 and 470.59 MHz, respectively, were measured under static conditions in the temperature range of −30 to 70 °C by the inversion recovery pulse sequence varying the recovery delay from 0.0001 to 2 s.

Low-field experiments were carried out on a Stelar PC-NMR spectrometer working at the ^{1}H and ^{19}F Larmor frequencies of 20.8 and 19.6 MHz, respectively, equipped with a single-channel static probe hosting standard glass tubes with an external diameter of 5 mm. The 90° pulse duration was 3.5 μs for both ^{1}H and ^{19}F. ^{1}H and ^{19}F spin−spin (T_2) and spin−lattice (T_1) relaxation times were measured in the temperature range of 26−100 °C. The temperature was controlled with an accuracy of 0.1 °C using air as the heating gas. ^{1}H T_1's were measured by the inversion recovery pulse sequence using recovery delays in the interval 0.01−3 s. For each delay, 8 scans were accumulated with a recycle delay of 3 s. ^{19}F T_1's were measured using the saturation recovery pulse sequence. Recovery curves were obtained using variable delays in the interval 0.001−5 s. For each delay, 32 scans were accumulated with a recycling delay of 0.1 s. At each temperature, the ^{1}H and ^{19}F recovery curves could be fitted by monoexponential functions. ^{1}H and ^{19}F on-resonance free induction decays (FIDs) were measured using the Magic Sandwich Echo (MSE) pulse sequence,[51] accumulating 400 scans and using recycle delays of 3 s for ^{1}H and 5 s for ^{19}F. ^{1}H and ^{19}F T_2 were determined by fitting the corresponding on-resonance FIDs with a linear combination of functions[52−55] as described in the Supporting Information.

2.4. Computational Methods. Q-Force[56] was used to derive molecule-specific force field parameters based on quantum mechanical (QM) data. All density functional theory (DFT) calculations were performed with the ORCA 5.0.4 computational package.[57,58] The ground-state geometry of a dimer was fully optimized with dispersion-corrected density functional theory using the B3LYP (D4) hybrid functional[59−61] and def2-SVP basis set[62] with the RIJCOSX auxiliary basis set.[63] Frequency calculations were executed to confirm that the optimized geometry was at a true minimum. For the construction of dihedral force field parameters with Q-Force, flexible dihedral scans (scan interval of 5°) were optimized under the composite electronic-structure method r^{2}SCAN-3c with no symmetry restrictions, and the def2-SVP basis set with the RIJCOSX auxiliary basis set was used for all single point energy calculations. The OPLS-AA force field[64] was used for all Lennard−Jones nonbonding parameters.

All-atomistic force field files and topologies were used to construct polymer chains and initial simulation boxes with the program Assemble!.[65] Partial charges for the polymer chains were calculated with ACC II using the charge equilibration method (QEq).[66]

GROMACS 2022.1[67] was used for all molecular dynamics simulations. Two simulation boxes were constructed. The first simulation box was packed according to the polymer concentrations in Table S1. The simulation box was equilibrated with 100 ps NVT and NPT simulations at 300 K and 1 bar, respectively, using the Bussi−Donadio−Parinello thermostat and Bernetti−Bussi barostat.[68,69] To further equilibrate, an annealing cycle was used where the simulation box was heated to 600 K and cooled back down to 300 K over the course of 1 ns, 10 times, for a total of 10 ns. A 15 ns production simulation at 300 K was used for the final visualization and data analysis. The second simulation box was packed with a single polymer chain containing 16 repeating units. After a 100 ps NVT equilibration, a 2 ns NVT production simulation was also performed. All simulations used a 2 fs time step and were visualized with a 1 ps time step.

3. RESULTS AND DISCUSSION

3.1. Synthesis, Physical, and Thermal Characterization of Polymers C1 and C1-d18. The synthesis of monomer **2** and polymer **C1-d18** is shown in Scheme 1. Polymer **C1-d18** only featured deuterated *t*-butyl groups, and the deuteration was performed first during *t*-butyl addition by refluxing *t*-butanol-d_{10} with anthracene in trifluoroacetic acid-d_1 to afford compound **1**.[70] Compound **1** and *p*-benzoquinone were refluxed with copper(I) chloride in glacial acetic acid to produce a triptycene-quinone Diels−Alder product that was tatutomerized, and treatment with sodium dithionite produced pure monomer **2**. Nucleophilic aromatic substitution polymerization of monomer **2**, or the nondeuterated analog (6,11-di(*tert*-butyl)triptycene-1,4-hydroquinone), with decafluorobiphenyl yielded polymers **C1-d18** and **C1**.[14] The molecular weight (M_n) and glass-transition temperature (T_g) of polymer **C1** (32.4 kDa and 298 °C, respectively) were similar to that of polymer **C1-d18** (31.9 kDa and 296 °C, respectively), confirming that the polymers are similar in structure (Table 1). Differential scanning calorimetry (DSC) was employed to measure glass-transition temperatures of both **C1** and **C1-d18** polymers (Table 1 and Figure S1). Size exclusion chromatography (SEC) was used to measure the molecular weights of both polymers (Table 1).

The BET surface area of polymer **C1** was measured to evaluate the porosity of the polymer. BET is typically used as an indirect measurement of microporosity. Figure 1 shows the BET isotherm of **C1** collected at 77 K under N_2. Polymer **C1** demonstrated IUPAC type I behavior with increasing pressure[71] and exhibited a BET surface area of 424 m^2 g^{-1}, which is in agreement with the BET isotherm and surface area reported for the higher-molecular-weight version of this polymer.[72]

3.2. Molecular Dynamics Simulations. MD simulations were used to investigate the reorientational motion of the methyl and *t*-butyl groups in the triptycene unit and the biphenyl moiety. A simulation box filled with a polydisperse selection of polymer chains and a simulation box containing a single polymer chain were constructed to study polymer chain

https://doi.org/10.1021/acs.macromol.4c02666
Macromolecules 2024, 57, 11152−11165

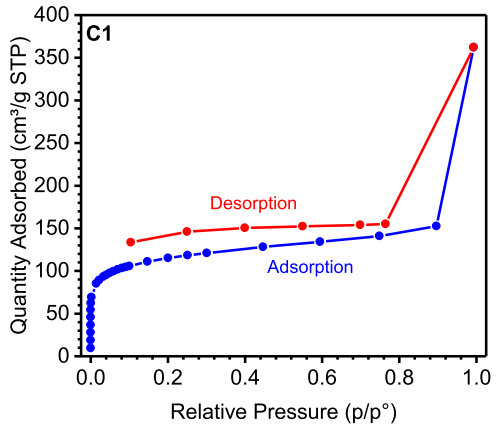

Figure 1. BET isotherm of polymer **C1** taken at 77 K with N_2.

movement (Figure 2). A simulation box packed with polymers allowed for the analysis of dynamics between tightly packed and entangled polymer chains. As a result of the overall homogeneity of the box, dynamics of polymers that would be located in less densely packed areas, such as large pores or sample edges, are not well described by the packed simulation box. A single polymer chain simulation allowed for visualization of unhindered movement and may be more indicative of how polymer chains in an experimental sample that would contain these areas of higher free volume could reorganize and move.

Flexible potential energy scans (PESs) from DFT computations for the methyl and *t*-butyl groups are depicted in Figure 3. As expected, in both cases, energy minima are observed at oscillation angles (φ) of 0, 120, 240, and 360°, in agreement with the 3-fold symmetry of these groups. Local minima are also present at φ = 60, 180, and 300°. Low and similar energy barriers between conformations were found for methyl (3−3.7 kJ/mol) and *t*-butyl groups (3 kJ/mol). Packed box and single polymer chain MD simulations showcase a combined rotation of rapidly rotating methyl groups and rotation of the entire *t*-butyl group (Figure 3). Furthermore, in the single-chain simulation, a reorientation of the triptycene group is noticeable. In the packed box simulation, this motion is less frequent due to steric effects from the entanglement of the surrounding polymer chains, but it is likely that in areas where polymer chains are not densely packed, this reorganization would be experimentally observable.

Additionally, MD simulations and PES analysis confirm one reorientational motion of the biphenyl moiety (Figure 4). Oscillation of the biphenyl ring occurs around the inter-ring C−C bond between the two twisted conformations of minimum energies at φ = 60 and 120°, where φ represents the dihedral angle between the planes of the two phenyl rings. This oscillation occurs with a small energy barrier of 5 kJ/mol, similar to the calculated energy barrier for the methyl- and *t*-butyl reorientations. The oscillation between the two phenyl rings passing through the φ = 90° conformation is observed in both packed box and single chain MD simulations but not through 180° where the energy barrier in the PES was calculated to be 129 kJ/mol.

3.3. Structural Characterization by ^{1}H, ^{19}F, and ^{13}C MAS NMR Spectra.

^{19}F and ^{1}H DE/MAS spectra of polymer **C1** are reported in Figure 5. In the ^{19}F DE/MAS spectrum (Figure 5a), there are two signals at −139.0 and −155.5 ppm with a 1:1 intensity ratio, ascribable to ^{19}F nuclei F-a and F-b of the biphenyl moiety, respectively.[73] The ^{1}H DE/MAS spectrum (Figure 5b) shows two signals at about 1.2 and 7.0 ppm, ascribable to the *t*-butyl and triptycene protons, respectively. In particular, from spectral deconvolution, we were able to discriminate between the signal of aromatic-H (7.3 ppm) and H-h (5.7 ppm) of the triptycene unit (inset of Figure 5b). The relative integrals of the observed signals are in good agreement with the monomer structure.

In Figure 6a, the ^{1}H−^{13}C and ^{19}F−^{13}C CP/MAS spectra of **C1** acquired with contact times (ct) of 1 and 7 ms, respectively, are shown. CP spectra recorded with other ct values are reported in Figure S2. In the ^{1}H−^{13}C CP/MAS spectrum, carbons belonging to the protonated unit can be selectively observed. Methyl carbons and quaternary carbons of *t*-butyl groups resonate at about 30.6 and 34.0 ppm, respectively. Signals of aromatic C−H and quaternary carbons of the triptycene group fall in the regions 109−130 and 132−148 ppm, respectively, whereas C-h can be observed at about 48 ppm. On the other hand, in the ^{19}F−^{13}C CP/MAS spectrum, signals of carbons belonging to the perfluorinated biphenyl moiety are favored. In the region between 139 and 145 ppm, the signals of C−F (C-a and C-b) and quaternary C-d carbons can be seen, while the quaternary C-c resonates at 102.9 ppm. The use of a long contact time (7 ms) was

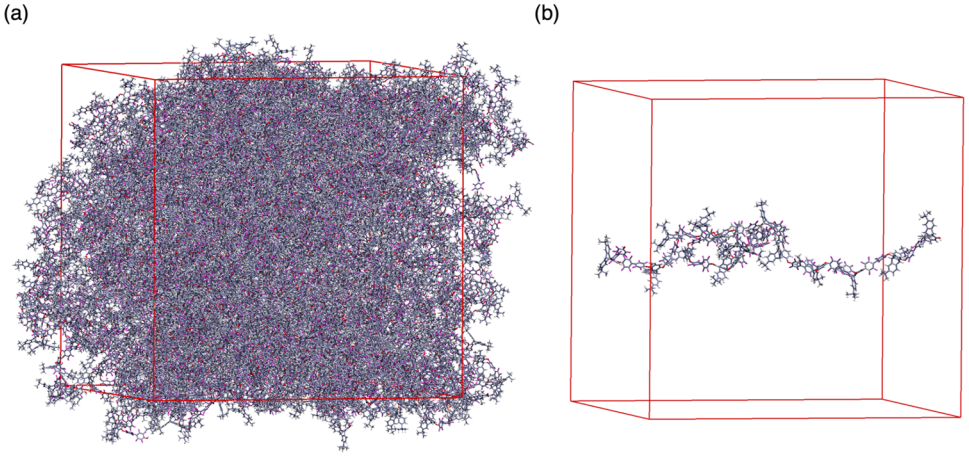

Figure 2. Simulation boxes of (a) packed polymer and (b) a single polymer chain.

https://doi.org/10.1021/acs.macromol.4c02666
Macromolecules 2024, 57, 11152−11165

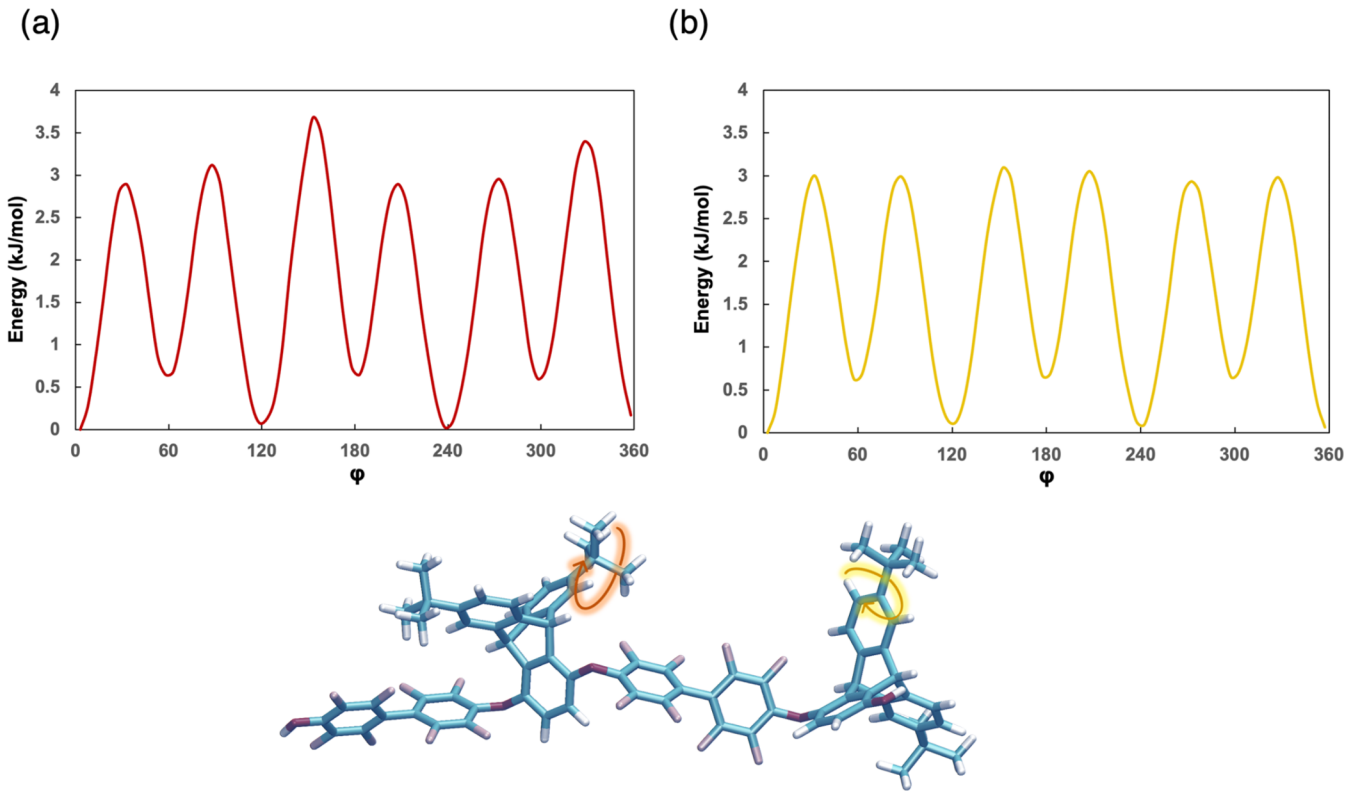

Figure 3. DFT PES scan of (a) methyl groups and (b) *t*-butyl groups.

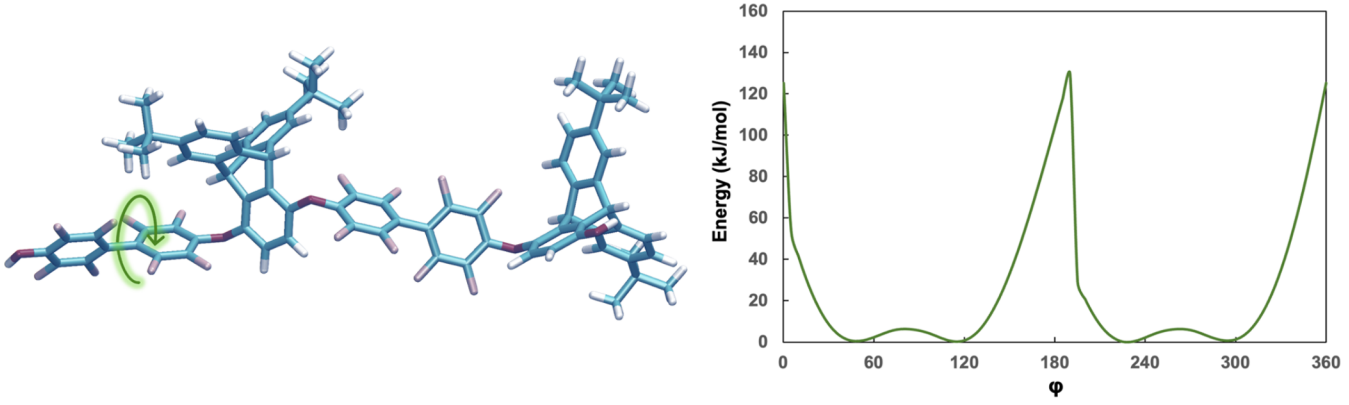

Figure 4. DFT PES scan of rotation around the biphenyl unit.

necessary to observe the signals of quaternary carbons C-c and C-d (~102 and 139 ppm), whose intensities increase by increasing the contact time as shown in Figure S2. The assignment of signals of C−F carbons was performed with the help of the 2D $^{19}F-^{13}C$ HETCOR spectrum reported in Figure 6b. It is observable that the ^{19}F signal at −155.5 ppm (F-a) correlates with the ^{13}C signal at about 142 ppm, which therefore can be assigned to C-a, while the ^{19}F signal at −139 ppm (F-b) correlates with the ^{13}C signal at 145 ppm, which can be assigned to C-b.

3.4. Dynamics Characterization by SSNMR. *3.4.1. Dynamics of Triptycene Moiety.* The dynamics of the triptycene unit was investigated by variable temperature measurements of spin−lattice relaxation times of ^1H nuclei ($T_1(^1H)$). $T_1(^1H)$ were measured at two different Larmor frequencies of 500.13 and 20.8 MHz. In both cases, ^1H $T_1(^1H)$ relaxation curves were found to be monoexponential in the whole investigated temperature range, with short $T_1(^1H)$ values (0.084−0.48 s at 500.13 MHz and 0.16−0.62 s at 20.8 MHz) increasing with temperature (Figure 7). $T_1(^{13}C)$'s of *t*-butyl and CH triptycene carbons were measured by $^1H-^{13}C$ CP/MAS Torchia experiments at the ^{13}C Larmor frequency of 125.77 MHz by integrating the spectral regions of the corresponding ^{13}C signals (Figure S3). The $T_1(^{13}C)$'s of the quaternary carbons of triptycene were not taken into account due to the overlap of signals in the region 130−160 ppm, making it difficult to accurately extract the integral.

The relaxation curves of all carbons were fitted by using single exponential functions. $T_1(^{13}C)$ was found to increase with temperature for all carbons as shown in Figure 7. Short $T_1(^{13}C)$ values were measured for both C-t (0.61−0.94 s) and C-s (6.7−10.4 s) *t*-butyl carbons, suggesting the proximity of a T_1 minimum in the low-temperature side of the investigated temperature interval. The increasing trends with temperature

https://doi.org/10.1021/acs.macromol.4c02666
Macromolecules 2024, 57, 11152−11165

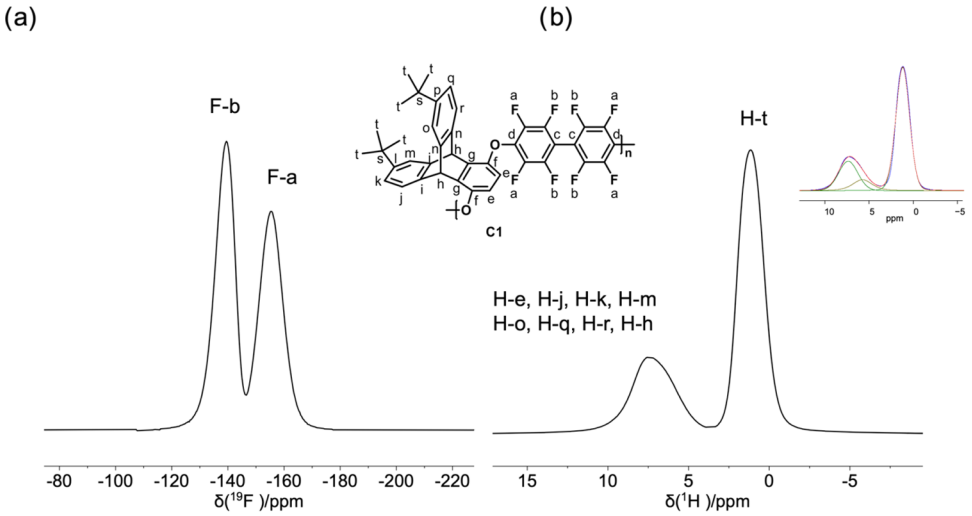

Figure 5. (a) ^{19}F and (b) ^{1}H MAS spectra of **C1**. The lettering reported here is used throughout the text.

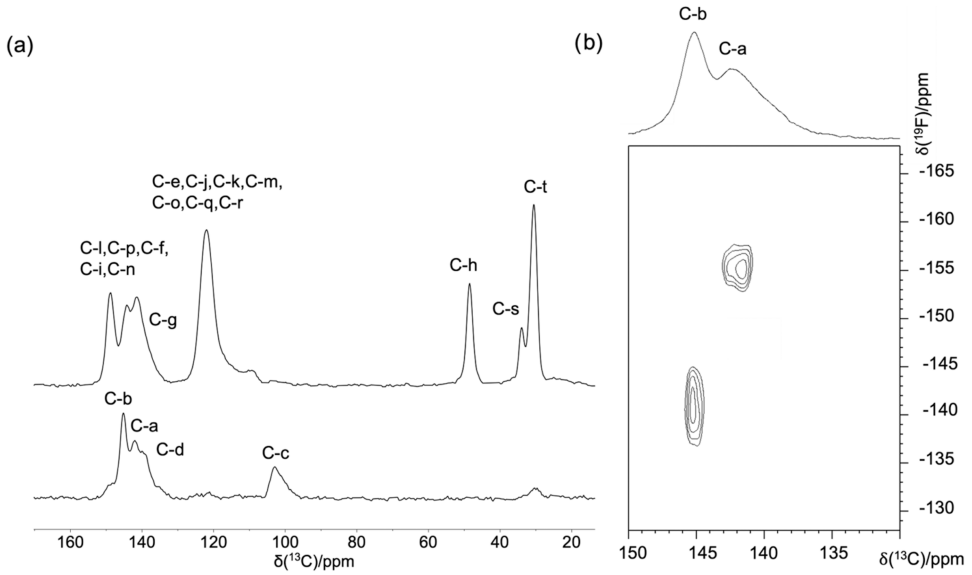

Figure 6. (a) ^{19}F−^{13}C CP/MAS spectrum (bottom) and ^{1}H−^{13}C CP/MAS spectrum (top), acquired with ct of 7 and 1 ms, respectively, of **C1**. (b) ^{19}F−^{13}C HETCOR spectrum of **C1** obtained with ct of 0.5 ms. The letters used for the assignment refer to the labeling reported in Figure 5.

observed for all of the measured $T_1(^1H)$ and $T_1(^{13}C)$ values indicate the presence of activated reorientational motions with characteristic frequencies in the fast MHz regime. These motions certainly include the fast rotation of the methyl groups about their ternary axis (C3) combined with a rotation of the whole *t*-butyl group around its ternary axis (C3′). Moreover, considering the increase in $T_1(^{13}C)$ of the C-h and CH aromatic triptycene carbons with temperature, a motion involving the triptycene group cannot be ruled out.

The presence of fast motions involving not only the methyl and *t*-butyl groups but also the whole triptycene group was confirmed by ^{1}H−^{13}C DIPSHIFT experiments, ^{1}H T_2 measurements, and ^{2}H static spectra. In DIPSHIFT experiments, the intensity of ^{13}C signal is measured as a function of an evolution time t_1, which is varied from 0 to one rotor period (T_{rot}) (see Section 3, Supporting Information). The obtained curves provide information on residual ^{1}H−^{13}C dipolar interactions as well as on the presence of motions with characteristic frequencies in the kHz regime. The experimental trends can be modeled using eqs S11a and S11b. The DIPSHIFT curves obtained at 25 °C for C-t, C-h, and CH aromatic carbons (Figure 8) show a symmetric trend with a minimum at $t_1 = T_{rot}/2$. This trend indicates the absence of motions in the intermediate kHz regime, which, if present, would cause a loss of signal intensity for long t_1's. On the other hand, the values of normalized intensity at the minimum, about 0.9 for C-t and 0.2−0.3 for C-h and CH carbons, reveal the presence of molecular motions in the fast regime, able to average the C−H dipolar couplings. The preaveraging factors *k*, estimated by fitting the curves to eq S11, are 0.01 for C-t and 0.5 for C-h. Factor *k* quantifies the extent to which the rigid dipolar second moment (M_2^{rigid}) is diminished due to fast dynamic processes.

The fitting was not performed for the curve of the CH aromatic carbons due to the superimposition of contributions from different nonequivalent carbons, which makes the interpretation more complicated. In the case of C-t, the estimated *k* value agrees with the preaveraging factor expected considering the fast three-site jump reorientations of the methyl and *t*-butyl groups about their 3-fold axes.[74,75]

https://doi.org/10.1021/acs.macromol.4c02666
Macromolecules 2024, 57, 11152−11165

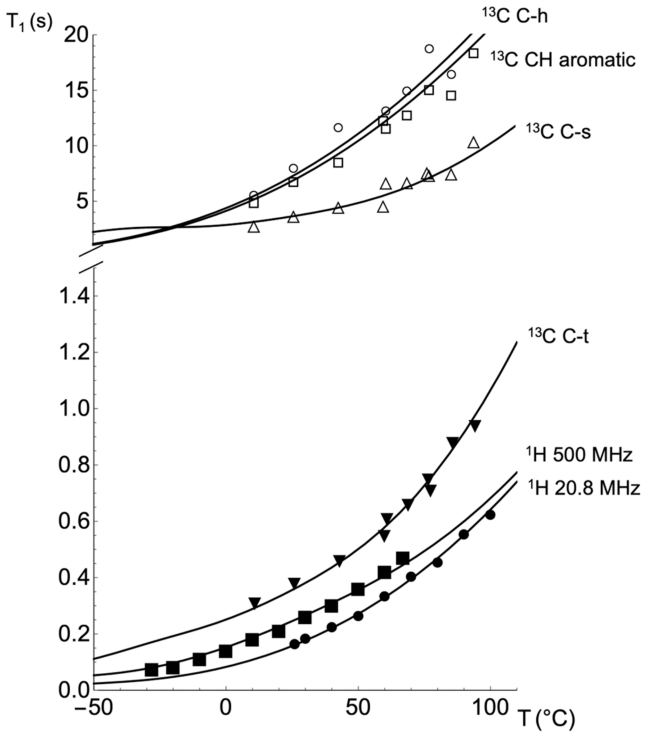

Figure 7. Experimental $T_1(^1H)$ *vs* temperature curves measured at the Larmor frequencies of 20.8 (black solid circles) and 500.13 MHz (black solid squares). Experimental $T_1(^{13}C)$ *vs* temperature curves measured at the Larmor frequency of 125.77 MHz: t methyl carbons (black down triangles), s quaternary carbons (open uptriangle), CH aromatic triptycene carbons (open squares), and h triptycene carbons (open circles). The black lines are the corresponding fitting functions, obtained as described later in the paper and in the Supporting Information.

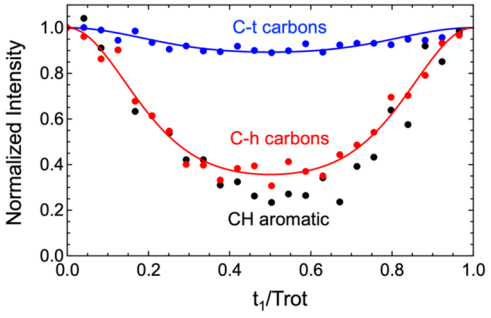

Figure 8. $^1H-^{13}C$ DIPSHIFT modulation curves of C-t carbons (blue points), C-h carbons (red points), and aromatic CH carbons (black points) at 25 °C. Solid lines correspond to the fitting curves. The normalized intensity was obtained by normalizing the intensity to the first point. DIPSHIFT curves of aromatic CH carbons were only treated qualitatively.

Interestingly, a slight decrease in k was observed by increasing the temperature from 0 to 50 °C (Figure S4a). This suggests the presence of additional motional processes reorienting the methyl groups, whose amplitude and/or rate increases with temperature in the explored range. For the C-h carbons, the low value of k estimated from the DIPSHIFT curves, which remains constant with temperature (Figure S4b), may result from a complex motion involving the reorientation of the triptycene unit about the C-f−C-f para axis combined with a "bending" of the C-f−O−C-d structure. This finding differs from the results of MD simulations, which did not reveal motions of the triptycene groups on the picosecond-to-nanosecond time scale in the simulation box with the polydisperse selection of polymer chains. This discrepancy might be due to differences in the arrangement of polymer chains in the actual sample. It is reasonable to expect that the real sample may possess a greater degree of free volume, allowing for increased motional freedom.

^1H apparent T_2's (T_2*) were also measured by fitting on-resonance ^1H FIDs recorded at variable temperature (Figure S5). ^1H T_2* was found to be 35 μs in the whole investigated temperature range, from which the value of the averaged homonuclear dipolar second moment ($M_2^{averaged}$) (Section 3, Supporting Information) could be determined through the relation $T_2^* = \sqrt{\frac{1}{8\pi M_2^{averaged}}}$. The obtained value was in line with the one calculated by considering the presence of fast reorientations of the methyl and t-butyl groups using the method reported in ref 76. This result suggests that the amplitude and/or geometry of the reorientational motions of the triptycene group are not effective in averaging the $^1H-^1H$ dipolar interaction.[77]

From the simulation of ^2H static spectra of **C1-d18** (Figure 9), an effective quadrupolar coupling constant, Q_{eff}, of ∼13.3

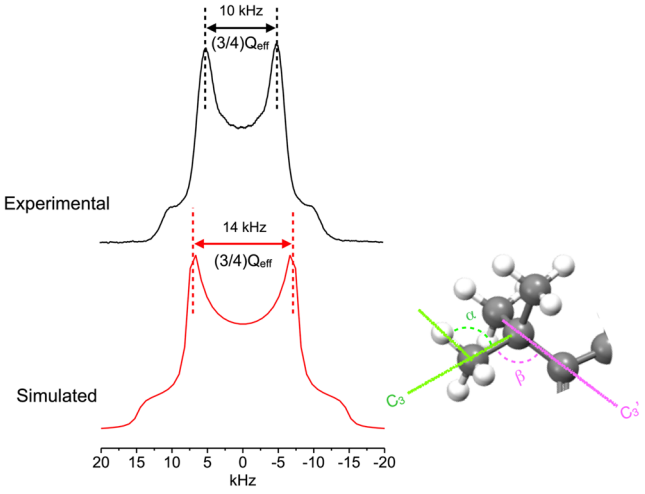

Figure 9. Top: experimental ^2H static line shape obtained for **C1-d18** at −28 °C. Bottom: simulated ^2H static line shape for ^2H nuclei belonging to t-butyl groups in the presence of fast uniaxial reorientations, in the extreme narrowing regime, of the CD_3 and t-butyl fragments about the C3 and C3′ 3-fold axes, as sketched on the right.

kHz was determined, which was found to be independent of temperature in the −28−70 °C interval. This value was lower than $Q_{eff}^{t\text{-}Bu}$ = 19.8 kHz predicted by eq S13, which considers two independent 3-site jump motions of the CD_3 groups about the C3 and C3′ axes (Figure 9).[78−80] This finding indicates the presence of an additional motion in the extreme narrowing regime, which results in further scaling of the quadrupolar interaction. This motion can be envisaged as the reorientation of the whole triptycene unit and/or a free diffusion in-a-cone motion of the t-butyl group.[78] However, it is worth noting that a slight deviation from the perfect tetrahedral geometry could also account for the small discrepancy between the experimental and theoretical values of Q_{eff}.

https://doi.org/10.1021/acs.macromol.4c02666
Macromolecules 2024, 57, 11152−11165

All of this considered, a global fitting of $T_1(^1H)$ and $T_1(^{13}C)$ measured at different temperatures was performed using the models described in Section 3, Supporting Information, in order to obtain quantitative information on the motion parameters. Specifically, it was assumed that the methyl and *t*-butyl reorientations about their ternary axes were the only motions in the fast MHz regime effective for the ^{13}C spin−lattice relaxation of C-s and C-t carbons, while aromatic CH and C-h carbons T_1's were fitted considering a motion involving the triptycene group. All of these motions were taken into account as effective for ^1H T_1 relaxation. The explicit equations used for fitting T_1's experimental values are reported in Section 6, Supporting Information. A good reproduction of the experimental trends was obtained (Figure 7), with the best fitting parameters reported in Tables 2 and S2. Notably, the

Table 2. Best-Fit Values of the Parameters of the Motions of the Methyl, *t*-Butyl, and Triptycene Groups as Obtained from the Analysis of the Variable Temperature $T_1(^1H)$ and $T_1(^{13}C)$ Data

fitting parameters	reorientation of the *t*-butyl groups	reorientation of the methyl groups	reorientation of the triptycene unit
E_a (kJ/mol)	20.8	15.8	13.7
$\log(\tau_\infty)$ (s)	−13	−13.5	−13.5
τ_c (ps) at 25 °C	452	19	7

optimized constants k^H, $k^{C\text{-}t}$, and $k^{C\text{-}s}$ (Table S2), obtained for $T_1(^1H)$ and $T_1(^{13}C)$ of C-t and C-s carbons, respectively, are compatible with the scaling of the $^1H-^1H$ and $^1H-^{13}C$ dipolar couplings due to the fast reorientation of the methyl groups.[81,82] As reported in Table 2, at 25 °C, the τ_c of methyl reorientation was found to be 19 ps, an order of magnitude shorter than that of *t*-butyl reorientation (τ_c = 452 ps). Similar activation energies (E_a) of 15.8 and 20.8 kJ/mol (Table 2) were obtained for the reorientations of methyl and *t*-butyl groups, respectively, in agreement with literature data.[83−86] These values are in good agreement with the interconformational energy barrier from the PES curves (Section 3.2). The experimental values of E_a are slightly larger than the calculated energy barriers between minimum-energy conformations, likely due to increased steric hindrance of the methyl and *t*-butyl moieties in the actual sample. The value of E_a obtained for the triptycene motion was 13.7 kJ/mol, with τ_c = 7 ps at 25 °C. The low values of E_a and τ_c, comparable to those obtained for the reorientation of the methyl groups, are quite unexpected for such a bulky group. This finding suggests that the detected motion consists of minor amplitude reorientations of the triptycene moiety, in agreement with the ^1H T_2* and ^2H spectra of the CD_3 groups (see above).

3.4.2. Dynamics of Biphenyl Moiety. A key dynamic feature to be investigated is the behavior of perfluorinated biphenyl groups. There are numerous examples where the motions of phenyl rings play a crucial role in determining the physicochemical properties of materials.[22,87,88] In a recent study, Brus et al. suggested that fast, small-amplitude fluctuations of aromatic linkers in MIL53(Al) for Li^+ batteries, detected via $^1H-^{13}C$ dipolar PILGRIM NMR spectroscopy, facilitate the transfer of Li^+ ions through the channel wall.[22] Additionally, flip motions of aromatic rings have been found to be sensitive to plasticization phenomena in glassy polymers.[87] While there are many studies in the literature on phenyl ring dynamics, knowledge about the motions of perfluorinated biphenyl groups, especially from experimental investigations, is limited. The substitution of hydrogen with fluorine may significantly alter both the conformational properties and dynamics.[89,90]

Similarly to what was done for the methyl, *t*-butyl, and triptycene groups, in this study the dynamics of the perfluorinated biphenyl linkers was characterized by the synergistic analysis of $T_1(^{19}F)$ and $T_1(^{13}C)$ relaxation times measured at variable temperature and $^{19}F-^{13}C$ DIPSHIFT experiments.

$T_1(^{19}F)$'s were measured at the two different Larmor frequencies of 470.59 and 19.6 MHz. In both cases, recovery curves displayed a monoexponential behavior in the whole investigated temperature range. Very short $T_1(^{19}F)$ values (0.076−0.52 s at 470.59 MHz and 0.31−0.89 s at 19.6 MHz) were obtained, increasing with temperature (Figure 10).

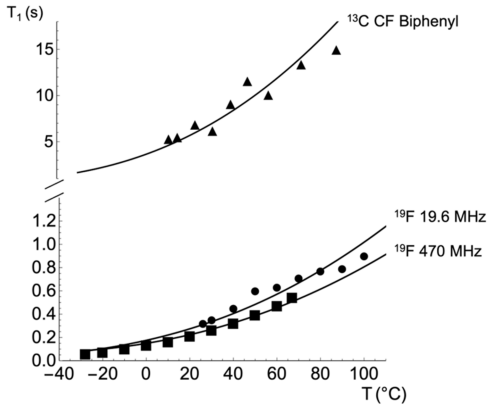

Figure 10. Experimental $T_1(^{19}F)$ curves *vs* temperature at the Larmor frequencies of 19.6 (black solid circles) and 470.59 MHz (black solid squares). Experimental $T_1(^{13}C)$ curves against temperature at a Larmor frequency of 125.77 MHz of fluorinated carbons (black solid uptriangles): a mean value was considered for (a) and (b). Black lines represent the corresponding fitting functions.

$T_1(^{13}C)$'s of the biphenyl moiety were selectively measured by means of Torchia experiments, exploiting cross-polarization from ^{19}F to ^{13}C nuclei. In particular, $T_1(^{13}C)$ of C-a and C-b were measured by extracting the corresponding recovery curves through a spectral deconvolution procedure (Figure S3). For both C-a and C-b, we obtained very similar $T_1(^{13}C)$ values, increasing with the temperature from 5.6 to 12.7 s (Figure 10). All in all, the results from $T_1(^{19}F)$ and $T_1(^{13}C)$, and in particular the observed increasing trends with temperature, clearly indicate that the biphenyl units undergo fast activated motions with characteristic frequencies on the order of MHz.

This finding was confirmed by the analysis of the $^{19}F-^{13}C$ DIPSHIFT curves (Figure 11). These curves display a symmetric trend, indicating the absence of motions in the kHz frequency regime and a value of normalized intensity at the minimum of about 0.7, independent of temperature over the investigated temperature range (Figure S4c). The fitting of the DIPSHIFT curves using eq S11 gave a value of the preaveraging factor *k* of 0.5. We can use the value of *k* to estimate the amplitude of the motions of the phenyl rings, considering the strength of the dipolar interaction between the CF carbons and the directly bonded ^{19}F nuclei as the "rigid"

https://doi.org/10.1021/acs.macromol.4c02666
Macromolecules 2024, 57, 11152−11165

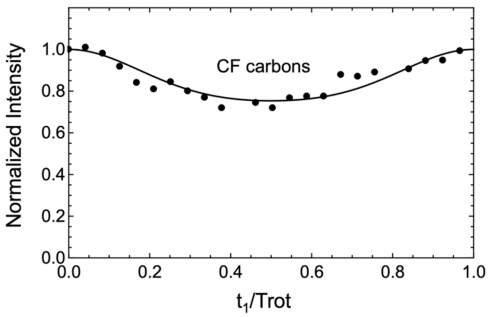

Figure 11. $^{19}F-^{13}C$ DIPSHIFT modulation curves of CF carbons obtained at 25 °C. Solid lines are the fitting curves. The normalized intensity was obtained by normalizing the intensity to the first point.

second moment M_2^{rigid} (eq S11). Simulations performed as described in ref 76 (Section 3, Supporting Information) showed that this value is compatible with the averaging of M_2^{rigid} by fast large amplitude oscillations of the biphenyl moiety around the inter-ring C−C bond of about 53°. Based on PES curves and MD simulations (Section 3.2), we attributed this motion to an activated oscillation of the biphenyl ring about the inter-ring C−C bond between the two twisted conformations of minimum energy, passing through the φ = 90° conformation. Moreover, the value of ^{19}F T_2* measured from the on-resonance ^{19}F FIDs (60 μs; Figure S6) in the whole investigated temperature range (26−100 °C) is in very good agreement with the value of ^{19}F $M_2^{averaged}$ calculated, considering the aforementioned biphenyl reorientation.

In order to get quantitative information on the parameters of the motion involving the biphenyl unit, we performed a simultaneous fitting of the $T_1(^{19}F)$ and $T_1(^{13}C)$ *vs* temperature curves by eqs S6 and S9, under the assumption that a single reorientational motion was present. In the case of ^{19}F nuclei, we also assumed that T_1 relaxation was determined by the fluctuations of $^{19}F-^{19}F$ homonuclear dipolar couplings. Although it is reasonable that the homonuclear dipolar interaction is the main source of relaxation, an additional contribution from ^{19}F chemical shift anisotropy[91] may also be present. A good reproduction of the experimental data was obtained with the best-fit functions and parameters reported in Figure 10 and Tables 3 and S3. The fitting gave an activation

Table 3. Best-Fit Values of the Parameters of the Motion of the Biphenyl Group as Obtained from the Analysis of Variable Temperature $T_1(^{19}F)$ and $T_1(^{13}C)$ Data

fitting parameters	reorientation of the biphenyl group
E_a (kJ/mol)	14.9
τ_c (ps) at 25 °C	30
$\log(\tau_\infty)$ (s)	−13

energy E_a of 14.9 kJ/mol for the biphenyl motion, corresponding to a correlation time of 30 ps at 25 °C. The value of E_a is in line with the small energy barrier between the two twisted conformations of minimum energy passing through the φ = 90° conformation predicted by PES curves (Figure 4) and previously obtained for perfluorinated biphenyl in the solid state.[90] Similarly to the case of methyl and *t*-butyl reorientations, the experimental value of E_a slightly exceeds the calculated energy barrier, probably due to an increased steric hindrance in the actual sample.

4. CONCLUSIONS

The SSNMR approach employed in this work, combining the synergistic analysis of multinuclear T_1 and T_2 relaxation data with DIPSHIFT experiments, supported by MD simulations, disclosed detailed insights into the local dynamics on the nanosecond-to-picosecond time scale of a FLARE porous polymer with potential application in gas separation membranes. Notably, experimental evidence for the dynamics of triptycene and perfluorinated biphenyl groups, previously unreported, was uncovered in this study.

Perfluorinated biphenyl groups undergo a fast reorientation about the inter-ring C−C bond between the two twisted minimum-energy conformations, passing through the conformation with the two phenyl rings arranged perpendicularly. A reorientation angle of about 53° and an activation energy of about 15 kJ/mol were found. In addition, fast reorientations of *t*-butyl groups bonded to the triptycene unit about the methyl and *t*-butyl ternary axes were detected together with fast small-amplitude reorientations of the "bulky" triptycene groups.

To the best of our knowledge, this study represents one of the first comprehensive investigations into the local dynamics of porous polymers for gas separation. The dynamic properties of these polymers and their correlation with performance remain largely unexplored, and further studies are needed to achieve a more complete understanding. The extensive insights gathered in this work could be leveraged in future research to investigate the role of dynamics in transport and separation mechanisms as well as in physical aging and plasticization phenomena, not only for the examined polymer but also for similar polymer-based membranes. To this end, in future studies, we will explore the impact of adsorbed gases on the observed motions, as well as how these dynamics evolve over time.

■ ASSOCIATED CONTENT

Supporting Information

The Supporting Information is available free of charge at https://pubs.acs.org/doi/10.1021/acs.macromol.4c02666.

Polymer concentrations in a packed simulation box used for molecular dynamics simulations. Differential scanning calorimetry measurements of **C1**; size exclusion chromatography experiments of **C1**; theoretical aspects of SSNMR experiments; $^{19}F-^{13}C$ and $^{1}H-^{13}C$ CP/MAS spectra of **C1** recorded with other contact times; $^{19}F-^{13}C$ and $^{1}H-^{13}C$ Torchia experiments; DIPSHIFT curves recorded at different temperatures; ^{1}H and ^{19}F T_2 relaxation time measurements; equations used for the fitting of spin−lattice relaxation curves as a function of temperature for the triptycene moiety; and additional parameters obtained from the fitting of spin−lattice relaxation curves (PDF)

■ AUTHOR INFORMATION

Corresponding Authors

Francesca Martini − *Dipartimento di Chimica e Chimica Industriale, Università di Pisa, 56124 Pisa, Italy; Istituto di Chimica dei Composti Organo Metallici, Consiglio Nazionale delle Ricerche (CNR-ICCOM), 56124 Pisa, Italy; Centro per l'Integrazione della Strumentazione Scientifica dell'Università di Pisa (CISUP), 56126 Pisa, Italy;*
Email: francesca.martini@unipi.it

https://doi.org/10.1021/acs.macromol.4c02666
Macromolecules 2024, 57, 11152−11165

Timothy M. Swager − *Department of Chemistry, Massachusetts Institute of Technology, Cambridge, Massachusetts 02139, United States;* orcid.org/0000-0002-3577-0510; Email: tswager@mit.edu

Authors

Elisa Della Latta − *Dipartimento di Chimica e Chimica Industriale, Università di Pisa, 56124 Pisa, Italy*

Kayla R. Storme − *Department of Chemistry, Massachusetts Institute of Technology, Cambridge, Massachusetts 02139, United States;* orcid.org/0000-0003-4520-9281

Molly C. Warndorf − *Department of Chemistry, Massachusetts Institute of Technology, Cambridge, Massachusetts 02139, United States;* orcid.org/0000-0002-0439-1550

Alfredo Alexander-Katz − *Department of Materials Science and Engineering, Massachusetts Institute of Technology, Cambridge, Massachusetts 02139, United States*

Silvia Borsacchi − *Istituto di Chimica dei Composti Organo Metallici, Consiglio Nazionale delle Ricerche (CNR-ICCOM), 56124 Pisa, Italy; Centro per l'Integrazione della Strumentazione Scientifica dell'Università di Pisa (CISUP), 56126 Pisa, Italy;* orcid.org/0000-0003-3696-0719

Marco Geppi − *Dipartimento di Chimica e Chimica Industriale, Università di Pisa, 56124 Pisa, Italy; Istituto di Chimica dei Composti Organo Metallici, Consiglio Nazionale delle Ricerche (CNR-ICCOM), 56124 Pisa, Italy; Centro per l'Integrazione della Strumentazione Scientifica dell'Università di Pisa (CISUP), 56126 Pisa, Italy;* orcid.org/0000-0002-2422-8400

Complete contact information is available at: https://pubs.acs.org/10.1021/acs.macromol.4c02666

Author Contributions

#E.D.L. and K.R.S. contributed equally. The manuscript was written through contributions of all authors. All authors have given approval to the final version of the manuscript.

Notes

The authors declare no competing financial interest.

■ ACKNOWLEDGMENTS

MISTI Global Seed Funds are acknowledged for the MIT-UNIPI project "Study of Porous Polymers for Gas Separation by NMR Spectroscopy", which provided partial financial support for this research and facilitated collaboration and exchange between the UNIPI and MIT groups. MIT also acknowledges the support of the National Science Foundation (DMR-2207299). Ministero dell'Università e della Ricerca (MUR) is acknowledged for the PRIN PNRR 2022 project "In-MoTion − Influence of Dynamics on the Adsorption and Transport Properties in Polymeric Materials for Membrane Technologies," funded by the European Union—Next Generation EU, which provided financial support for this research. CISUP (Center for Instrument Sharing-University of Pisa) is acknowledged for the use of the Bruker Avance Neo 500 solid-state NMR spectrometer.

■ ABBREVIATIONS

BET, Brunauer−Emmett−Teller; BPP, Bloembergen−Purcell−Pound; CP, cross-polarization; ct, contact time; DE, direct excitation; DFT, density functional theory; DIPSHIFT, dipolar chemical shift correlation; DSC, differential scanning calorimetry; E_a, activation energy; FFV, fractional free volume; FID, free induction decay; FLARE, fluorinated aryl ethers; FSLG, frequency-switched Lee−Goldburg; GPC, gel permeation chromatography; HETCOR, heteronuclear correlation; HPLC, high-performance liquid chromatography; HRMS (DART-TOF), high-resolution mass spectrometry (direct analysis in real-time-time-of-flight); LG, Lee−Goldburg; M_2, second moment; MAS, magic angle spinning; MD, molecular dynamics; M_n, molecular weight; MOFs, metal organic frameworks; MSE, magic sandwich echo; NMR, nuclear magnetic resonance; PDI, molecular weight distribution; PESs, potential energy scans; PWRA, population weighted rate average; Q_0, quadrupolar coupling constant; Q_{eff}, effective quadrupolar coupling constant; QM, quantum mechanical; R_1, spin−lattice relaxation rate; S, order parameter; SEC, size exclusion chromatography; S_NAr, nucleophilic aromatic substitution; SSNMR, solid-state NMR; T_1, spin−lattice relaxation time; t_1, evolution time; T_2, spin−spin relaxation time; T_2*, apparent spin−spin relaxation time; τ_c, correlation time; T_g, glass-transition temperature; T_{rot}, rotor period; VT, variable temperatures

■ REFERENCES

(1) Galizia, M.; Chi, W. S.; Smith, Z. P.; Merkel, T. C.; Baker, R. W.; Freeman, B. D. 50th Anniversary Perspective: Polymers and Mixed Matrix Membranes for Gas and Vapor Separation: A Review and Prospective Opportunities. *Macromolecules* **2017**, *50* (20), 7809−7843.

(2) Sanders, D. F.; Smith, Z. P.; Guo, R.; Robeson, L. M.; McGrath, J. E.; Paul, D. R.; Freeman, B. D. Energy-Efficient Polymeric Gas Separation Membranes for a Sustainable Future: A Review. *Polymer* **2013**, *54* (18), 4729−4761.

(3) Sholl, D. S.; Lively, R. P. Seven Chemical Separations to Change the World. *Nature* **2016**, *532*, 435−437.

(4) Robeson, L. M. Correlation of Separation Factor versus Permeability for Polymeric Membranes. *J. Membr. Sci.* **1991**, *62* (2), 165−185.

(5) Merkel, T. C.; Pinnau, I.; Prabhakar, R.; Freeman, B. D.Gas and Vapor Transport Properties of Perfluoropolymers. In *Materials Science of Membranes for Gas and Vapor Separation*; Wiley, 2006; pp 251−270.

(6) Smith, Z. P.; Tiwari, R. R.; Dose, M. E.; Gleason, K. L.; Murphy, T. M.; Sanders, D. F.; Gunawan, G.; Robeson, L. M.; Paul, D. R.; Freeman, B. D. Influence of Diffusivity and Sorption on Helium and Hydrogen Separations in Hydrocarbon, Silicon, and Fluorocarbon-Based Polymers. *Macromolecules* **2014**, *47* (9), 3170−3184.

(7) Wu, A. X.; Drayton, J. A.; Smith, Z. P. The Perfluoropolymer Upper Bound. *AIChE J.* **2019**, *65* (12), No. e16700, DOI: 10.1002/aic.16700.

(8) Wu, A. X.; Drayton, J. A.; Rodriguez, K. M.; Qian, Q.; Lin, S.; Smith, Z. P. Influence of Aliphatic and Aromatic Fluorine Groups on Gas Permeability and Morphology of Fluorinated Polyimide Films. *Macromolecules* **2020**, *53* (13), 5085−5095.

(9) Scott, R. L. The Anomalous Behavior of Fluorocarbon Solutions. *J. Phys. Chem. A* **1958**, *62* (2), 136−145.

(10) Song, W.; Rossky, P. J.; Maroncelli, M. Modeling Alkane +perfluoroalkane Interactions Using All-Atom Potentials: Failure of the Usual Combining Rules. *J. Chem. Phys.* **2003**, *119* (17), 9145−9162.

(11) Yee, A. F.; Smith, S. A. Molecular structure effects on the dynamic mechanical spectra of polycarbonates. *Macromolecules* **1981**, *14* (1), 54−64.

(12) Zhang, Y.; Geng, Z.; Niu, S.; Zhang, S.; Luan, J.; Wang, G. Preparation and Applications of Low-Dielectric Constant Poly Aryl Ether. *Adv. Ind. Eng. Polym. Res.* **2020**, *3* (4), 175−185.

(13) Boyer, R. F. *Molecular Basis of Transitions and Relaxations*; CRC Press, 1978; Vol. *4*.

(14) Long, T. M.; Swager, T. M. Molecular Design of Free Volume as a Route to Low-κ Dielectric Materials. *J. Am. Chem. Soc.* **2003**, *125* (46), 14113−14119.
(15) Smith, S. J. D.; Hou, R.; Konstas, K.; Akram, A.; Lau, C. H.; Hill, M. R. Control of Physical Aging in Super-Glassy Polymer Mixed Matrix Membranes. *Acc. Chem. Res.* **2020**, *53* (7), 1381−1388.
(16) Lau, C. H.; Mulet, X.; Konstas, K.; Doherty, C. M.; Sani, M. A.; Separovic, F.; Hill, M. R.; Wood, C. D. Hypercrosslinked Additives for Ageless Gas-Separation Membranes. *Angew. Chem., Int. Ed.* **2016**, *55* (6), 1998−2001.
(17) Sefcik, M. D.; Schaefer, J. Solid-state ^{13}C NMR evidence for gas−polymer interactions in the carbon dioxide−poly(vinyl chloride) system. *J. Polym. Sci., Polym. Phys. Ed.* **1983**, *21* (7), 1055−1062.
(18) Perego, J.; Bezuidenhout, C. X.; Bracco, S.; Prando, G.; Marchiò, L.; Negroni, M.; Carretta, P.; Sozzani, P.; Comotti, A. Cascade Dynamics of Multiple Molecular Rotors in a MOF: Benchmark Mobility at a Few Kelvins and Dynamics Control by CO_2. *J. Am. Chem. Soc.* **2021**, *143* (33), 13082−13090.
(19) Bracco, S.; Castiglioni, F.; Comotti, A.; Galli, S.; Negroni, M.; Maspero, A.; Sozzani, P. Ultrafast Molecular Rotors and Their CO_2 Tuning in MOFs with Rod-Like Ligands. *Chem. − Eur. J.* **2017**, *23* (47), 11210−11215.
(20) Murdock, C. R.; McNutt, N. W.; Keffer, D. J.; Jenkins, D. M. Rotating Phenyl Rings as a Guest-Dependent Switch in Two-Dimensional Metal-Organic Frameworks. *J. Am. Chem. Soc.* **2014**, *136* (2), 671−678.
(21) Perego, J.; Bezuidenhout, C.; Pedrini, A.; Bracco, S.; Negroni, M.; Comotti, A.; Sozzani, P. Reorientable fluorinated aryl rings in triangular channel Fe-MOFs: an investigation on CO_2−matrix interactions. *J. Mater. Chem. A* **2020**, *8*, 11406−11413.
(22) Brus, J.; Czernek, J.; Urbanova, M.; Rohlíček, J.; Plecháček, T. Transferring Lithium Ions in the Nanochannels of Flexible Metal-Organic Frameworks Featuring Superchaotropic Metallacarborane Guests: Mechanism of Ionic Conductivity at Atomic Resolution. *ACS Appl. Mater. Interfaces* **2020**, *12* (42), 47447−47456.
(23) Zorn, R.; Lohstroh, W.; Zamponi, M.; Harrison, W. J.; Budd, P. M.; Böhning, M.; Schönhals, A. Molecular Mobility of a Polymer of Intrinsic Microporosity Revealed by Quasielastic Neutron Scattering. *Macromolecules* **2020**, *53*, 6731−6739.
(24) Inoue, R.; Kanaya, T.; Masuda, T.; Nishida, K.; Yamamuro, O. Relationship between the Local Dynamics and Gas Permeability of Para-Substituted Poly(1-chloro-2-phenylacetylenes). *Macromolecules* **2012**, *45*, 6008−6014.
(25) Kanaya, T.; Teraguchib, M.; Masudab, T.; Kajia, K. Local mobility of substituted polyacetylenes measured by quasielastic neutron scattering and its relationship with gas permeability. *Polymer* **1999**, *40*, 7157−7161.
(26) Kanaya, T.; Tsukushi, I.; Kaji, K.; Sakaguchi, T.; Kwak, G.; Masuda, T. Role of Local Dynamics in the Gas Permeability of Glassy Substituted Polyacetylenes. A Quasielastic Neutron Scattering Study. *Macromolecules* **2002**, *35*, 5559−5564.
(27) Guan, H.; Li, J.; Zhou, T.; Pang, Z.; Fu, Y.; Cornelio, J.; Wang, Q.; Telfer, S. G.; Kong, X. Probing Nonuniform Adsorption in Multicomponent Metal−Organic Frameworks via Segmental Dynamics by Solid-State Nuclear Magnetic Resonance. *J. Phys. Chem. Lett.* **2020**, *11*, 7167−7176.
(28) Gonzalez-Nelson, A.; Coudert, F.-X.; van der Veen, M. A. Rotational Dynamics of Linkers in Metal−Organic Frameworks. *Nanomaterials* **2019**, *9*, 330.
(29) Khudozhitkov, A. E.; Jobic, H.; Kolokolov, D. I.; Freude, D.; Haase, J.; Stepanov, A. G. Probing the Guest-Mediated Structural Mobility in the UiO-66(Zr) Framework by ^2H NMR Spectroscopy. *J. Phys. Chem. C* **2017**, *121*, 11593−11600.
(30) Wong, Y. T. A.; Martins, V.; Lucier, B. E. G.; Huang, Y. Solid-State NMR Spectroscopy: A Powerful Technique to Directly Study Small Gas Molecules Adsorbed in Metal−Organic Frameworks. *Chem. − Eur. J.* **2019**, *25*, 1848−1853.
(31) Nardelli, F.; Nerli, F.; Della Latta, E.; Martini, F.; Geppi, M.; Taddei, M.; Calucci, L. Unveiling CO_2 Dynamics in Perfluorinated Cerium-Based Metal−Organic Frameworks with UiO-66 and MIL-140 Topologies by Solid State NMR. *J. Phys. Chem. C* **2024**, *128* (16), 6887−6896.
(32) Smith, P. B.; Moll, D. J. Deuterium NMR investigation of the plasticization effects induced by high-pressure carbon dioxide gas on the molecular dynamics of polymers. *Macromolecules* **1990**, *23* (13), 3250−3256.
(33) Hill, A. J.; Pas, S. J.; Bastow, T. J.; Burgar, M. I.; Nagai, K.; Toy, L. G.; Freeman, B. D. Influence of Methanol Conditioning and Physical Aging on Carbon Spin-Lattice Relaxation Times of Poly(1-Trimethylsilyl-1-Propyne). *J. Membr. Sci.* **2004**, *243* (1−2), 37−44.
(34) Williams, R.; Burt, L. A.; Esposito, E.; Jansen, J. C.; Tocci, E.; Rizzuto, C.; Lanč, M.; Carta, M.; McKeown, N. B. A Highly Rigid and Gas Selective Methanopentacene-Based Polymer of Intrinsic Microporosity Derived from Tröger's Base Polymerization. *J. Mater. Chem. A* **2018**, *6* (14), 5661−5667.
(35) Bezzu, C. G.; Carta, M.; Ferrari, M. C.; Jansen, J. C.; Monteleone, M.; Esposito, E.; Fuoco, A.; Hart, K.; Liyana-Arachchi, T. P.; Colina, C. M.; McKeown, N. B. The Synthesis, Chain-Packing Simulation and Long-Term Gas Permeability of Highly Selective Spirobifluorene-Based Polymers of Intrinsic Microporosity. *J. Mater. Chem. A* **2018**, *6* (22), 10507−10514.
(36) Song, Q.; Cao, S.; Pritchard, R. H.; Ghalei, B.; Al-Muhtaseb, S. A.; Terentjev, E. M.; Cheetham, A. K.; Sivaniah, E. Controlled Thermal Oxidative Crosslinking of Polymers of Intrinsic Microporosity towards Tunable Molecular Sieve Membranes. *Nat. Commun.* **2014**, *5*, No. 4813.
(37) Heuchel, M.; Fritsch, D.; Budd, P. M.; McKeown, N. B.; Hofmann, D. Atomistic Packing Model and Free Volume Distribution of a Polymer with Intrinsic Microporosity (PIM-1). *J. Membr. Sci.* **2008**, *318* (1−2), 84−99.
(38) Yi, S.; Ghanem, B.; Liu, Y.; Pinnau, I.; Koros, W. J. Ultraselective Glassy Polymer Membranes with Unprecedented Performance for Energy-Efficient Sour Gas Separation. *Sci. Adv.* **2019**, *5* (5), No. eaaw5459.
(39) Fang, W.; Zhang, L.; Jiang, J. Polymers of Intrinsic Microporosity for Gas Permeation: A Molecular Simulation Study. *Mol. Simul.* **2010**, *36* (12), 992−1003.
(40) Rukmani, S. J.; Liyana-Arachchi, T. P.; Hart, K. E.; Colina, C. M. Ionic-Functionalized Polymers of Intrinsic Microporosity for Gas Separation Applications. *Langmuir* **2018**, *34* (13), 3949−3960.
(41) Zhou, J.; Zhu, X.; Hu, J.; Liu, H.; Hu, Y.; Jiang, J. Mechanistic Insight into Highly Efficient Gas Permeation and Separation in a Shape-Persistent Ladder Polymer Membrane. *Phys. Chem. Chem. Phys.* **2014**, *16* (13), 6075−6083.
(42) Fang, W.; Zhang, L.; Jiang, J. Gas Permeation and Separation in Functionalized Polymers of Intrinsic Microporosity: A Combination of Molecular Simulations and Ab Initio Calculations. *J. Phys. Chem. C* **2011**, *115*, 14123−14130.
(43) Rodríguez-González, F. E.; Soto, C.; Palacio, L.; Montero-Alejo, A. L.; Escalona, N.; Schott, E.; Comesaña-Gándara, B.; Terraza, C. A.; Tundidor-Camba, A. Polymers of Intrinsic Microporosity Containing Aryl-Phthalimide Moieties: Synthesis, Modeling, and Membrane Gas Transport Properties. *Polym. Chem.* **2023**, *14* (19), 2363−2373.
(44) Ma, B.; Chen, C.; Du, Z. X.; Zhang, L. Effect of Oxygen Atoms and Cyano Groups on Mixed Gas Separation of PIM-1 Membranes: MD Simulations. *J. Mol. Liq.* **2023**, *386*, No. 122362.
(45) Mazlan, N.; Jusoh, N.; Sow Mun Lock, S. Investigation of Transport Properties of 6FDA-Durene Polymeric Membrane for Landfill Gas Application Using Molecular Simulation Approach. *Chemosphere* **2022**, *307* (P3), No. 136019.
(46) DeAzevedo, E. R.; Saalwachter, K.; Pascui, O.; De Souza, A. A.; Bonagamba, T. J.; Reichert, D. Intermediate Motions as Studied by Solid-State Separated Local Field NMR Experiments. *J. Chem. Phys.* **2008**, *128* (10), No. 104505.
(47) Cobo, M. F.; Achilles, A.; Reichert, D.; DeAzevedo, E. R.; Saalwächter, K. Recoupled Separated-Local-Field Experiments and

https://doi.org/10.1021/acs.macromol.4c02666
Macromolecules 2024, 57, 11152−11165

Applications to Study Intermediate-Regime Molecular Motions. *J. Magn. Reson.* **2012**, *221*, 85−96.
(48) Fung, B. M.; Khitrin, A. K.; Ermolaev, K. An Improved Broadband Decoupling Sequence for Liquid Crystals and Solids. *J. Magn. Reson.* **2000**, *142* (1), 97−101.
(49) Van Rossum, B. J.; Förster, H.; De Groot, H. J. M. High-Field and High-Speed CP-MAS ^{13}C NMR Heteronuclear Dipolar-Correlation Spectroscopy of Solids with Frequency-Switched Lee-Goldburg Homonuclear Decoupling. *J. Magn. Reson.* **1997**, *124* (2), 516−519.
(50) Torchia, D. A. The Measurement of Proton-Enhanced Carbon-13 T_1 Values by a Method Which Suppresses Artifacts. *J. Magn. Reson.* **1978**, *30* (3), 613−616.
(51) Rhim, W. K.; Pines, A.; Waugh, J. S. Time-Reversal Experiments in Dipolar-Coupled Spin Systems. *Phys. Rev. B* **1971**, *3*, 684−696.
(52) Pierigé, M.; Nardelli, F.; Calucci, L.; Cettolin, M.; Giannini, L.; Causa, A.; Martini, F.; Geppi, M. Exploring the Effect of Resins of Different Origin on the Structure, Dynamics and Curing Characteristics of SBR Compounds. *Polymers* **2024**, *16* (6), 834.
(53) Della Latta, E.; Sabatini, F.; Micheletti, C.; Carlotti, M.; Martini, F.; Nardelli, F.; Battisti, A.; Degano, I.; Geppi, M.; Pucci, A.; Pohl, S.; Kickelbick, G. Performant Flexible Luminescent Solar Concentrators of Phenylpolysiloxanes Crosslinked with Perylene Bisimide Fluorophores. *Polym. Chem.* **2023**, *14* (14), 1602−1612.
(54) Nardelli, F.; Martini, F.; Lee, J.; Lluvears-Tenorio, A.; La Nasa, J.; Duce, C.; Ormsby, B.; Geppi, M.; Bonaduce, I. The Stability of Paintings and the Molecular Structure of the Oil Paint Polymeric Network. *Sci. Rep.* **2021**, *11* (1), No. 14202.
(55) Nardelli, F.; Calucci, L.; Carignani, E.; Borsacchi, S.; Cettolin, M.; Arimondi, M.; Giannini, L.; Geppi, M.; Martini, F. Influence of Sulfur-Curing Conditions on the Dynamics and Crosslinking of Rubber Networks: A Time-Domain NMR Study. *Polymers* **2022**, *14* (4), 767.
(56) Sami, S.; Menger, M. F. S. J.; Faraji, S.; Broer, R.; Havenith, R. W. A. Q-Force: Quantum Mechanically Augmented Molecular Force Fields. *J. Chem. Theory Comput.* **2021**, *17* (8), 4946−4960.
(57) Neese, F.; Wennmohs, F.; Becker, U.; Riplinger, C. The ORCA Quantum Chemistry Program Package. *J. Chem. Phys.* **2020**, *152* (22), No. 224108.
(58) Neese, F. Software Update: The ORCA Program System—Version 5.0. *Wiley Interdiscip. Rev. Comput. Mol. Sci.* **2022**, *12* (5), No. e1606.
(59) Becke, A. D. Density-functional Thermochemistry. III. The Role of Exact Exchange. *J. Chem. Phys.* **1993**, *98* (7), 5648−5652.
(60) Lee, C.; Yang, W.; Parr, R. G. Development of the Colle-Salvetti Correlation-Energy Formula into a Functional of the Electron Density. *Phys. Rev. B* **1988**, *37* (2), 785.
(61) Caldeweyher, E.; Ehlert, S.; Hansen, A.; Neugebauer, H.; Spicher, S.; Bannwarth, C.; Grimme, S. A Generally Applicable Atomic-Charge Dependent London Dispersion Correction. *J. Chem. Phys.* **2019**, *150* (15), No. 154122.
(62) Weigend, F.; Ahlrichs, R. Balanced Basis Sets of Split Valence, Triple Zeta Valence and Quadruple Zeta Valence Quality for H to Rn: Design and Assessment of Accuracy. *Phys. Chem. Chem. Phys.* **2005**, *7* (18), 3297−3305.
(63) Helmich-Paris, B.; de Souza, B.; Neese, F.; Izsák, R. An Improved Chain of Spheres for Exchange Algorithm. *J. Chem. Phys.* **2021**, *155* (10), No. 104109.
(64) Jorgensen, W. L.; Maxwell, D. S.; Tirado-Rives, J. Development and Testing of the OPLS All-Atom Force Field on Conformational Energetics and Properties of Organic Liquids. *J. Am. Chem. Soc.* **1996**, *118* (45), 11225−11236.
(65) Degiacomi, M. T.; Erastova, V.; Wilson, M. R. Easy Creation of Polymeric Systems for Molecular Dynamics with Assemble! *Comput. Phys. Commun.* **2016**, *202*, 304−309.
(66) Raček, T.; Schindler, O.; Toušek, D.; Horský, V.; Berka, K.; Koča, J.; Svobodová, R. Atomic Charge Calculator II: Web-Based Tool for the Calculation of Partial Atomic Charges. *Nucleic Acids Res.* **2020**, *48* (W1), W591−W596.
(67) Abraham, M. J.; Murtola, T.; Schulz, R.; Páll, S.; Smith, J. C.; Hess, B.; Lindah, E. GROMACS: High Performance Molecular Simulations through Multi-Level Parallelism from Laptops to Supercomputers. *SoftwareX* **2015**, *1−2*, 19−25.
(68) Bussi, G.; Donadio, D.; Parrinello, M. Canonical Sampling through Velocity Rescaling. *J. Chem. Phys.* **2007**, *126* (1), 14101.
(69) Bernetti, M.; Bussi, G. Pressure Control Using Stochastic Cell Rescaling. *J. Chem. Phys.* **2020**, *153* (11), No. 114107.
(70) Fu, P. P.; Harvey, R. G. Synthesis and Rearrangement of *tert*-Butylanthracene. *J. Org. Chem.* **1977**, *42* (14), 2407−2410.
(71) Thommes, M.; Kaneko, K.; Neimark, A. V.; Olivier, J. P.; Rodriguez-Reinoso, F.; Rouquerol, J.; Sing, K. S. W. Physisorption of Gases, with Special Reference to the Evaluation of Surface Area and Pore Size Distribution (IUPAC Technical Report). *Pure Appl. Chem.* **2015**, *87* (9−10), 1051−1069.
(72) Storme, K. R.; Schreib, B. S.; Smith, Z. P.; Swager, T. M. Tuning Porosity in Triptycene-Poly(arylene ether)s. *Macromolecules* **2024**, *57*, 7533−7546.
(73) Tie, W.; Zhong, Z.; Wen, P.; Lee, M. H.; Li, X. D. Synthesis and characterization of a novel photocrosslinkable fluorinate poly-(arylene ether) for optical waveguide. *Mater. Lett.* **2009**, *63*, 1381−1383.
(74) Palmer, A. G.; Williams, J.; McDermott, A. Nuclear Magnetic Resonance Studies of Biopolymer Dynamics. *J. Phys. Chem. A* **1996**, *100* (31), 13293−13310.
(75) Lorieau, J.; McDermott, A. E. Order Parameters Based on $^{13}C^1H$, $^{13}C^1H_2$ and $^{13}C^1H_3$ Heteronuclear Dipolar Powder Patterns: A Comparison of MAS-Based Solid-State NMR Sequences. *Magn. Reson. Chem.* **2006**, *44* (3), 334−347.
(76) Goc, R. Computer calculation of the Van Vleck second moment for materials with internal rotation of spin groups. *Comput. Phys. Commun.* **2004**, *162*, 102−112.
(77) Müller, K.; Geppi, M. *Solid State NMR: Principles, Methods, and Applications*, 1st ed.; Wiley-VCH: Weinheim, Germany, 2021; pp 397−445.
(78) Stepanov, A. G.; Alkaev, M. M.; Shubin, A. A. Molecular Dynamics of Iso-Butyl Alcohol inside Zeolite H-ZSM-5 as Studied by Deuterium Solid-State NMR Spectroscopy. *J. Phys. Chem. B* **2000**, *104* (32), 7677−7685.
(79) Mantsch, H. H.; Saitô, H.; Smith, I. C. P. Deuterium Magnetic Resonance, Applications in Chemistry, Physics and Biology. *Prog. Nucl. Magn. Reson. Spectrosc.* **1977**, *11* (4), 211−272.
(80) Nishchenko, A. M.; Kolokolov, D. I.; Stepanov, A. G. Mobility of Solid Tert -Butyl Alcohol Studied by Deuterium NMR. *J. Phys. Chem. A* **2011**, *115* (26), 7428−7436.
(81) Beckmann, P. A.; Buser, C. A.; Gullifer, K.; Mallory, F. B.; Mallory, C. W.; Rossi, G. M.; Rheingold, A. L. Methyl and T-Butyl Group Reorientation in Planar Aromatic Solids: Low-Frequency Nuclear Magnetic Resonance Relaxometry and x-Ray Diffraction. *J. Chem. Phys.* **2003**, *118* (24), 11129−11138.
(82) Riddell, F. G.; Arumugam, S.; Harris, K. D. M.; Rogerson, M.; Strange, J. H. A ^{13}C CP/MAS NMR Study of a Double tert-Butyl Group Rotation in the Solid State Using T_1, and Line Shape Measurements. *J. Am. Chem. Soc.* **1993**, *115* (5), 1881−1885.
(83) Popa, L. C.; Rheingold, A. L.; Beckmann, P. A. A Proton Spin-Lattice Relaxation Rate Study of Methyl and t-Butyl Group Reorientation in the Solid State. *Solid State Nucl. Magn. Reson.* **2010**, *38* (1), 31−35.
(84) Beckmann, P. A.; McGhie, A. R.; Rheingold, A. L.; Sloan, G. J.; Szewczyk, S. T. Solid-Solid Phase Transitions and Tert-Butyl and Methyl Group Rotation in an Organic Solid: X-Ray Diffractometry, Differential Scanning Calorimetry, and Solid-State ^{1}H Nuclear Spin Relaxation. *J. Phys. Chem. A* **2017**, *121* (33), 6220−6230.
(85) Scarperi, A.; Carignani, E.; Martini, F.; Embs, J. P.; Wąsicki, J.; Barcaro, G.; Geppi, M.; Pajzderska, A. Different Dynamic Behavior of Methyl Groups in Crystalline Carbimazole as Revealed by a

https://doi.org/10.1021/acs.macromol.4c02666
Macromolecules 2024, 57, 11152−11165

Multitechnique Experimental and Theoretical Approach. *J. Phys. Chem. C* **2023**, *127* (10), 5186−5196.
(86) Carignani, E.; Borsacchi, S.; Geppi, M. Dynamics by Solid-State NMR: Detailed Study of Ibuprofen Na Salt and Comparison with Ibuprofen. *J. Phys. Chem. A* **2011**, *115* (32), 8783−8790.
(87) Spiess, H. W. Molecular Dynamics of Solid Polymers as Revealed by Deuteron NMR. *Colloid Polym. Sci.* **1983**, *261* (3), 193−209.
(88) Schmidt-Rohr, K. R.; Clause, J.; Spiess, H. W. Correlation of Structure, Mobility, and Morphological Information in Heterogeneous Polymer Materials by Two-Dimensional Wideline-Separation NMR Spectroscopy. *Macromolecules* **1992**, *25* (12), 3273−3277.
(89) Fahey, D. P.; Dougherty, W. G.; Kassel, W. S.; Wang, X.; Beckmann, P. A. Nonexponential Solid State 1H and 19F Spin−Lattice Relaxation, Single-crystal X-ray Diffraction, and Isolated-Molecule and Cluster Electronic Structure Calculations in an Organic Solid: Coupled Methyl Group Rotation and Methoxy Group Libration in 4,4′- Dimethoxyoctafluorobipheny. *J. Phys. Chem. A* **2012**, *116*, 11946−11956.
(90) Grein, F. Twist Angles and Rotational Energy Barriers of Biphenyl and Substituted Biphenyls. *J. Phys. Chem. A* **2002**, *106* (15), 3823−3827.
(91) Martini, F.; Miah, H. K.; Iuga, D.; Geppi, M.; Titman, J. J. Measuring 19F Shift Anisotropies and ^{1}H-^{19}F Dipolar Interactions with Ultrafast MAS NMR. *J. Magn. Reson.* **2015**, *259*, 102−107.

https://doi.org/10.1021/acs.macromol.4c02666
Macromolecules 2024, 57, 11152−11165